

¹ **Spatio-temporal scaling of hydrological and**
² **agrochemical export dynamics in a tile-drained**
³ **Midwestern watershed**

K. Guan¹, S.E. Thompson², C. J. Harman³, N. B. Basu⁴, P. S. C. Rao⁵, M.

Sivapalan^{3,6,7}, A. I. Packman⁸, P. K. Kalita⁹

4 **Abstract.** Conceptualizing catchments as physico-chemical filters is an
5 appealing way to link streamflow discharge and concentration timeseries to
6 hydrological and biogeochemical processing in hillslopes and drainage net-
7 works. Making these links explicit is challenging in complex watersheds, but

K. Guan, Department of Civil and Environmental Engineering, Princeton University, Princeton, New Jersey, USA, (kguan@princeton.edu)

S.E. Thompson, Nicholas School of the Environment, Duke University, Durham, NC, 27707,(set8@duke.edu), currently at School of Civil Engineering, Purdue University (Corresponding Author)

C. Harman, Department of Civil and Environmental Engineering, University of Illinois at Urbana-Champaign, Champaign, Illinois, USA, (charman2@illinois.edu)

N. Basu, Department of Civil Engineering, University of Iowa, Iowa City, Iowa, USA, (nandita-basu@uiowa.edu)

P. Suresh C. Rao, School of Civil and Environmental Engineering, Purdue University, Purdue, Indiana, USA, (pscr@purdue.edu)

M. Sivapalan, Department of Civil and Environmental Engineering, University of Illinois at Urbana-Champaign, Champaign, Illinois, USA, (sivapala@illinois.edu)

A. I. Packman, Department of Civil Engineering, Northwestern University, Evanston, Illinois, USA, (a-packman@northwestern.edu)

P. K. Kalita, Department of Agricultural and Biological Engineering, University of Illinois at Urbana-Champaign, Champaign, Illinois, USA, (pkalita@illinois.edu)

¹Department of Civil and Environmental

8 may be possible in highly modified catchments where hydrological and bio-
9 geochemical processes are simplified. Linking hydrological and biogeochem-
10 ical filtering in highly modified watersheds is appealing from a water qual-
11 ity perspective in order to identify the major controls on chemical export at
12 different spatial and temporal scales. This study investigates filtering using
13 a 10-year dataset of hydrological and biogeochemical export from a small (<

Engineering, Princeton

²Nicholas School of the Environment,
Duke University

³Department of Civil and Environmental
Engineering, UIUC

⁴Department of Civil Engineering and
Environmental, University of Iowa

⁵School of Civil Engineering and
Agronomy Department, Purdue University

⁶Department of Geography, UIUC

⁷Department of Water Management, Delft
University of Technology

⁸Department of Civil Engineering,
Northwestern University

⁹Department of Agriculture and
Biological Engineering, UIUC

14 500km²) agricultural watershed in Illinois, the Little Vermilion River (LVR)
15 Watershed. A number of distinct scaling regimes were identified in the Fourier
16 power spectrum of discharge and nitrate, phosphate and atrazine concentra-
17 tions. These scaling regimes were related to different runoff pathways and
18 spatial scales throughout the catchment (surface drainage, tile drains and
19 channel flow in the river). Wavelet analysis indicated increased coupling be-
20 tween discharge and in-stream concentrations at seasonal-annual timescales.
21 Using a multi-resolution analysis nitrate, phosphate and atrazine loads ex-
22 ported at annual scales were found to exhibit near-linear scaling with annual
23 streamflow, suggesting that at these scales the export dynamics could be ap-
24 proximated as chemostatic responses. This behavior was pronounced for ni-
25 trate and less so for phosphate and atrazine. The analysis suggests that bio-
26 geochemical inputs built up legacy loads, leading to the emergence of chemo-
27 static behavior at annual timescales, even at the relatively small scale of the
28 LVR.

1. Introduction: Catchments as physico-chemical filters

29 The conceptualization of hydrological systems as a cascade of hierarchical filters, trans-
30 forming an input signal of rainfall [*Matsoukas et al.*, 2000], through infiltration [*Meng*
31 *et al.*, 2006], and the water table [*Li and Zhang*, 2007] to produce a streamflow response
32 [*Sauquet et al.*, 2008], has a growing history in statistical hydrology [*Tessier et al.*, 1996].
33 This area of study has focused on the timeseries features of hydrological signatures, in
34 particular with respect to their multifractal properties, the emergence of multiple scaling
35 regimes, and the consequences for prediction of extreme events [*Schertzer et al.*, 2006].
36 Rainfall drives the generation of hydrological responses in catchments, and so it is rea-
37 sonable to expect that the resulting hydrological signatures should inherit the scaling
38 properties of rainfall, smoothed to varying extents depending upon filtering due to soil-
39 water deficits induced by ET losses, and the resulting distribution of residence times in
40 the system [*Zhou et al.*, 2006]. This smoothing can be isolated (in some cases) as the
41 transfer function that converts the input signature into an output, and this transfer func-
42 tion represents the hydrological filtering action of the catchment [*Schertzer et al.*, 2006].
43 However, a unique transfer function approach may not always be applicable, especially
44 in highly transient systems where catchment residence time distributions are time-varient
45 [*Majone et al.*, 2010].

46 Treating catchments as hydrological filters offers an alternative conceptualization to
47 either detailed, distributed process modeling, or lumped, whole-catchment ‘black box’
48 models. The body of existing studies on catchments as filters, however, could be extended
49 in two significant ways. Firstly the properties of filtering in the catchment could be

50 linked more explicitly to the underlying mechanistic processes of rainfall-runoff response
51 [*Kirchner*, 2009]. Secondly, hydrological fluxes drive many other critical functions of
52 watersheds including biogeochemical processing, ecological functioning and the utility of
53 ecosystems for human exploitation.

54 While the role of a catchment as a hydrologic filter has been relatively well explored in
55 different contexts, biogeochemical ‘filtering’ as driven by the catchment hydrology has only
56 recently begun to receive equal attention, in part due to the difficulties associated with
57 collecting high resolution timeseries of export over sufficiently long periods of time [*Kirch-*
58 *ner et al.*, 2004; *Godsey et al.*, 2010]. Much of the interest in understanding the temporal
59 scaling of solute concentrations has been driven by studies of conservative tracers which
60 can offer insight into travel time distributions of water in the catchment [*Kirchner et al.*,
61 2000, 2001; *Godsey et al.*, 2010]. Spectral techniques have been used to infer retardation
62 constants for atmospherically derived tracers [*Feng et al.*, 2004a], and to explore the signa-
63 tures of nitrogen transport [*Zhang and Schilling*, 2005]. Broader questions relating to the
64 interplay of biogeochemical reactivity, biological uptake and release, retardation processes
65 and transport pathways as drivers of catchment biogeochemistry, and their reflection in
66 the scaling properties of stream biogeochemistry largely remain to be addressed. A com-
67 bination of field studies and simulations suggest that processes occurring within shallow
68 saturated zones [*Zhang and Schilling*, 2004], karstic or fractured aquifers [*Majone et al.*,
69 2004], hyporheic zones [*Cardenas*, 2008] and the vadose zone [*Feng et al.*, 2004a] can all
70 contribute to observed power-law scaling of biogeochemical export and in-stream concen-
71 trations. Given the potential complexity of both hydrological [*Botter et al.*, 2010], and
72 biogeochemical filtering processes, inference linking filtering to physico-chemical mecha-

73 nisms is most feasible in catchments with simple hydrology. Even in relatively simple
74 systems, it has been argued that explicit observation of individual flow paths is needed to
75 make reasonable predictions about solute transport [*Rozemeijer et al.*, 2010a].

76 The tile drained watersheds of the Midwestern US present ideal examples of such simpli-
77 fied catchments. Contemporary Midwestern landscapes are essentially human creations,
78 reflecting an almost complete conversion of natural prairies, wetlands and forests to crop-
79 lands. Vast tracts of land ($\sim 75\%$) or approximately a 500,000 km² area, are planted to
80 corn-soybean rotation. The hydrology of the Midwestern landscapes has been extensively
81 modified to promote rapid drainage, primarily by the construction of extensive networks of
82 artificial drainage (surface ditches and subsurface tile drains) [*Basu et al.*, 2010a; *Schilling*
83 *and Helmers*, 2008]. The artificial drainage network increases the hydrological connectiv-
84 ity of the landscape to the channels, allowing flows to bypass much of the complexity of
85 the landscape. This promotes spatial homogeneity in runoff generation, leading to flashy
86 responses to rainfall and exponential recession curves which dominate flow in the artificial
87 drainage network and the streams [*Evans and Fausey*, 1999; *Basu et al.*, 2010a]. Further,
88 in these watersheds, the application of fertilizers, pesticides, and animal manures has sig-
89 nificantly perturbed the natural biogeochemical regime. The application of agrochemicals
90 has impacted water quality at both the local scale, across the basin as a whole, and in
91 receiving water bodies, most dramatically in driving coastal hypoxia in the Gulf of Mexico
92 [*Rabalais et al.*, 2002; *Phillips et al.*, 2006; *Blann et al.*, 2009; *McLaughlin and Mineau*,
93 1995].

94 The water quality impacts of agricultural drainage are driven by the exported chemical
95 mass load (L), typically computed as the product of concentration (C) and the discharge

96 rate (Q). Variation and covariation of C and Q are both important controls on the dy-
97 namics of L [Borsuk *et al.*, 2004]. In a recent analysis of agricultural watersheds from
98 around the world, Basu *et al.* [2010b] demonstrated that loads of total nitrogen and to-
99 tal phosphorus were well approximated as a linear function of Q at large spatial scales
100 and annual timescales. This implies that the annually flow-weighted value of C was es-
101 sentially constant, a phenomenon we will refer to here as ‘chemostatic behavior’. For
102 smaller, unmanaged catchments, and at all timescales, Godsey *et al.* [2009] showed that
103 chemostatic behavior provided an excellent description of the export dynamics of a range
104 of geologically derived solutes. Basu *et al.* [2010b] hypothesized that the chemostatic be-
105 havior of nutrients in large basins arose from legacy effects: namely the large accumulated
106 stores of N and P in agricultural landscapes. As a result, these anthropogenic compounds
107 behaved analogously to geologically derived species such as calcium or magnesium salts.
108 A secondary question motivating the study of hydrological and biogeochemical filtering
109 in agricultural watersheds, then, is to ascertain the spatio-temporal scale dependence of
110 chemostatic behavior, and the possible determinants of such dependence.

111 Of course, despite the simplicity of an agricultural catchment in comparison to unman-
112 aged catchments, the catchments are nonetheless dynamic, and much of the dynamism
113 is driven by intensive management practice and seasonal cycles of crop planting, growth
114 and harvest. For example, crop growth cycles have an important effect on the seasonal
115 changes in the uptake of water and nutrients from the root zone, as influenced by the
116 changes over time in the depth-distribution of roots and the maximum rooting depth.
117 Thus, the crop-available amount of water and nutrients increase from late spring through
118 the summer growing season, as the root zone increases. Crop uptake represents a large

119 sink for both water and nutrients, and the periodicity of this uptake is anticipated to
120 contribute to the function of the catchment as a filter.

121 In this study, we investigate the spatio-temporal variation and covariation of C , Q and
122 L for three agrochemicals: nitrate (NO_3^-), phosphate (PO_4^{3-}) and atrazine. The study
123 analyzes these dynamics within a small ($< 500\text{km}^2$) agricultural watershed in Eastern Illi-
124 nois, the Little Vermilion River Watershed (LVR), which exhibits the simplifying features
125 (dense artificial drainage networks, relatively homogeneous cropping and anthropogenic
126 chemical loading) typical of Midwestern landscapes. The three agrochemicals display dif-
127 ferent chemical properties in terms of both reactivity and sorption, allowing the effects
128 of these properties on the emergent filtering to be examined together. The study aims to
129 address three guiding questions:

- 130 1. What are the characteristics of the hydrological and biogeochemical filters operating
131 in the LVR?
- 132 2. Can the properties of these filters be used to ‘fingerprint’ different reactive transport
133 processes? and
- 134 3. On what spatial and temporal scales are chemostatic responses observed?

135 These questions are largely addressed through a series of analyses in the frequency do-
136 main, documented in the methods section below. Frequency domain analysis is naturally
137 motivated by the filtering concept, which deconvolves the action of different linear filters,
138 simplifying the analysis. Scaling features that are difficult to distinguish in the time do-
139 main are exaggerated in the frequency domain, facilitating comparisons across different
140 sites, scales and solutes [Godsey *et al.*, 2010]. Finally, frequency domain techniques al-
141 low the variability and correlation behavior of timeseries to be compared and isolated at

142 different temporal scales, making them well suited to an examination of the temporal de-
143 pendence of chemostatic behavior. The conceptual understanding obtained by addressing
144 the research questions is ultimately synthesized to generate a conceptual model of solute
145 filtering by the landscape of the Little Vermilion River Watershed.

2. Methods

2.1. Study location and data collection

146 The Little Vermilion River Watershed (LVR) (see Figure 1 for a map), is located in
147 Eastern Illinois, USA ($40^{\circ}06'21.45''N$, $87^{\circ}41'34.12''W$) [Mitchell *et al.*, 2000]. The LVR
148 watershed has a drainage area of about 489 km², generally flat topography with slopes < 1
149 degree and primarily silty- or silty clay loam soils. Approximately 90% of the watershed
150 is devoted to intensive agricultural production and is cropped under a corn- soybean
151 rotation, typical of many Midwestern agricultural watersheds [Algoazany, 2006]. Mean
152 annual precipitation is approximately 1,040 mm [Algoazany, 2006]. The hydrology in
153 the watershed has been highly modified by the construction of an extensive network of
154 irregularly-spaced subsurface tile drains and surface drainage ditches, which discharge to
155 stream channels. Subsurface drainage dominates the water budget because of the flat
156 topography, with surface runoff being important only during infrequent high-intensity
157 events during early spring when the soil water content is at its maximum [Mitchell *et al.*,
158 2000]. On average, subsurface runoff represents more than 90% of the total flow. The
159 dominance of the tile-drains is also reflected in the chemical export, at least for nitrate and
160 atrazine, 99.5% and 96% of which (respectively) are exported via this pathway. Phosphate,
161 however, is disproportionately represented in the surface flow paths, which accounted for
162 between 28 and 58% of export in the drainage areas studied [Algoazany, 2006]. This

163 partitioning is attributable to strong phosphate sorption on fine particulate matter which
164 is readily exported during surface runoff events.

165 The data used in this study are from a 10-year (1991-2000) project monitoring hydro-
166 logical variability and water quality in the LVR [*Algoazany, 2006*]. Hydrological fluxes
167 (rainfall and stream flow) were recorded continuously, with flow sampling occurring on
168 15 minute intervals [*Mitchell et al., 2000*]. Chemical constituents, including nitrate, phos-
169 phate and a number of pesticides were recorded using a stratified sampling design. During
170 low flow periods chemical sampling was undertaken every 14 days. Above a site-specific
171 flow threshold (summarized in Table 1) higher frequency sampling (typically at 5 hour
172 intervals) was undertaken. Loads were computed by interpolating concentration data be-
173 tween measurements and using the high frequency flow data. The load data were linearly
174 interpolated to give a daily load timeseries which was used for the frequency analysis.
175 Although *Rozemeijer et al.* [2010b] found that using sparse concentration data could lead
176 to significant errors in computed loads, this estimate was based on a weekly sampling
177 regime. By contrast, the higher frequency within-storm sampling undertaken at the Lit-
178 tle Vermillion River allows for several concentrations measurements to be made during
179 significant storm events, avoiding the gross biases found by *Rozemeijer et al.* [2010b].
180 Measurement techniques are described in *Algoazany* [2006]. Measurements were taken at
181 a range of spatial scales (local tile drainage areas and several points in the main river
182 channel) so that the contributing areas sampled span three orders of magnitude (see Ta-
183 ble 1). Each of the local drainage areas had 2 monitoring stations, one for the tile drain,
184 and the other the surface drains. This study focuses on three co-located tile and surface
185 drainage stations (denoted A_1/A_2 , B_1/B_2 and C_1/C_2 , where 1 indicates a subsurface tile

186 drain and \mathcal{D} indicates a surface drain), and two river gauges (R_3 and R_5). Note that the
187 R_5 station is located in the upper catchment and has a smaller drainage area than R_3
188 (see Figure 1). Detailed data on the timing of agricultural management practices (e.g.
189 fertilizer and herbicide application) were collected for the area around tile-flow stations
190 A_1 and B_1 in order to investigate the influence of land-management on chemical transport
191 at small scales [Algoazany, 2006].

2.2. Biogeochemistry of nitrate, phosphate and atrazine

192 In the LVR, the patterns of chemical concentration observed in streamflow can be con-
193 ceptualized as arising from an interplay between processes that remove chemicals from
194 transport in flow, and processes which renew the availability of the solutes for such trans-
195 port. Renewal processes include natural biogeochemical cycling (weathering, nitrification
196 etc.), but are dominated by the application of fertilizers and pesticides. Removal from
197 transport may occur due to several different processes including reversible transformation
198 (e.g. complexation or mineralization), irreversible transformations (e.g. denitrification
199 and volatilization), plant or microbial uptake, or sorption onto soil / colloidal particles.
200 In general, we may characterize the reactivity of species by a reaction constant, or, equiv-
201 alently for first order reactions, a half-life. Sorption of different chemicals is represented
202 by an effective sorption coefficient, K_d (L^3/M): admittedly this is a simplification of much
203 more complex models for sorption dynamics [Brusseau and Rao, 1989], particularly in the
204 case of phosphate. The chemicals considered here each have different biological, physical
205 and chemical pathways that remove them from being available for aqueous transport.
206 Simplified reaction formulations are useful because they allow cross-comparison of the
207 overall behavior of disparate chemicals during the period of observation.

208 Of the three solutes analyzed in this paper, nitrate is not significantly sorbed ($K_d \sim 0$),
209 atrazine is weakly sorbing ($K_{oc} = 100L/kg$, or $K_d \sim 1 L/kg$ for soils with 1 – 2% organic
210 content, [Wauchope *et al.*, 1992]) and phosphorous strongly sorbed ($K_d \sim 330 - 5150$
211 L/kg, [Machesky *et al.*, 2010]). The phosphorus species analyzed in the LVR is soluble,
212 dissolved inorganic P (PO_4^{3-}). However phosphate in the aqueous phase is in equilibrium
213 with the sorbed phases (particulate P). We thus expect the phosphate export dynamics
214 to reflect the dynamics of particulate P to a large extent. Soluble atrazine dynamics
215 may weakly reflect the transport of bound atrazine, and nitrate dynamics should be
216 essentially independent of particle movement. The potential for particle-bound transport
217 to be important for strongly sorbing species may have significant implications for the
218 dominant transport processes both on the soil surface and in the vadose zone, with fast
219 flow pathways (overland or preferential flow in macropores or cracks) representing an
220 increased fraction of the export for highly sorbing species [McGrath, 2007]. The reactivity
221 of the solutes determines to first order how long the solute can persist in the catchment
222 in the absence of transport. Atrazine has a documented half life of ~ 60 days [Wauchope
223 *et al.*, 1992]. Reactivity is difficult to estimate for N and P due to internal cycling in
224 association with microbiological and plant uptake. The potential for sorptive, uptake and
225 reactive processes to result in relatively short-lived signals of export in the stream following
226 application to the landscape drives the choice of renewal and removal from transport as
227 the most general descriptors of chemical processing.

2.3. Load-discharge and concentration-discharge relationships

228 Several data analysis techniques were employed to explore the relationships between
229 concentration C , discharge Q and the exported mass loads L . The initial analysis consisted

230 of comparing the spectral properties of discharge and the exported concentration in the
231 Fourier domain. Wavelet analysis was used to compute the wavelet coherence for the L - Q
232 and Q - C signals. Finally, a multi-resolution analysis was used to filter the timeseries and
233 allow L - Q relationships to be investigated as a function of different averaging windows in
234 the time domain. These methods are described in detail below.

235 **2.3.1. Fourier spectral analysis**

236 Fourier analysis begins with transforming a timeseries $X(t)$ from the time (t) domain
237 into the frequency (f) (see Equation 1). The transformed timeseries are most conveniently
238 viewed in terms of their power-spectrum, $|X(f)|^2$ (normalized to have variance equal
239 to 1), which shows how the variance of the timeseries is partitioned amongst different
240 frequencies [Katul *et al.*, 2007]. Peaks in the power spectrum are indicative of strongly
241 periodic signals in the timeseries. Flat regions in the power spectrum are referred to as
242 ‘white noise’ in which variability occurs equivalently on all timescales. When the power
243 spectrum is viewed on a log-log scale, linear regions often appear, indicating power-law
244 scaling across a range of frequencies, i.e. $|X(f)|^2 \sim f^{-\alpha}$ [Harris *et al.*, 1997]. The slope
245 of such linear regions is often related to processes that induce statistically self-similar
246 behavior [Fraedrich and Larnder, 1993]. Usually such scaling behavior is restricted to
247 a range of frequencies, corresponding to the scales over which the self-similar processes
248 operate (Figure 2 (A) and (B)).

249 We examined scaling behavior in flow at different sites in the LVR to investigate hydro-
250 logical filtering (i.e. transformation of rainfall signals into discharge) in the watershed. To
251 isolate the effect of this filtering, we normalized the power spectrum of flow by that of the
252 rainfall. Estimation of the exponent α for different power-law regimes, and of the breaks in

253 scaling between these regimes is complicated by the fact that power spectra are typically
 254 noisy. To avoid errors in fitting due to this noise, we used an octave binning algorithm
 255 as a smoothing technique to allow a robust fit. Unlike the traditional window smoothing
 256 method, which may result in heavily biased scaling exponent estimation towards the high
 257 frequency end of the spectra, octave binning divides the power spectrum into logarithmic
 258 frequency bins, and calculates the mean and variance of the power spectrum within each
 259 bin, thus avoiding any bias between frequencies (see details in [*Fraedrich and Larnder,*
 260 1993]). Linear fitting via least squares regression to these bins allows the estimation of α
 261 for each scaling range [*Harris et al., 1997*]. We determined the existence of break points
 262 in the spectra by fitting over progressively larger ranges of bins and determining when
 263 the addition of the next bin would result in a statistically significant change in the slope
 264 of the regression (see Figure 2: C,D,E). The Fourier Transform and linear fitting were
 265 applied to the timeseries of flow, load and concentration in the LVR dataset.

266 Fourier analysis also offers a direct insight into the question of chemostatic response
 267 and $L - Q$ linearity. The Fourier transform of L is given by:

$$L(f) = \int_{-\infty}^{\infty} \exp(ift) \mathbf{C} \times Q(t) dt = C_c Q(f) \quad (1)$$

268 where we have assumed that C_c is a constant (and therefore distinct from C , the timeseries
 269 of concentration). That is:

$$C_c^2 = \frac{|L(f)|^2}{|Q(f)|^2} \quad (2)$$

270 If the ratio determined from Equation 2 deviates from white noise then we must reject
 271 the hypothesis that C_c is invariant, because we will have identified scales over which

272 C_c changes in a self-similar fashion. Such an invalidation does not necessarily imply that
273 these variations in C_c contribute to variation in load to the same extent as variations in Q ,
274 because this frequency-based analysis does not account for the magnitude of fluctuations.
275 Similarly, white noise scaling in C_c does not necessarily imply that C_c is independent of
276 Q , since the noise in C_c may reflect that in Q [Feng *et al.*, 2004b]. Consequently, analysis
277 based on Equation 2 is primarily concerned with the identification of timescales on which
278 processes acting against chemostatic behavior might occur.

279 Spectral analysis in the Little Vermilion River is complicated by the fact that the
280 surface drainage is highly intermittent in comparison to the tile drains, and the tile drains
281 themselves are ephemeral, frequently ceasing to flow in late summer. Although no-flow
282 periods were included in the analysis because the Fourier Transform technique requires
283 continuous data, the power spectrum of the flow and concentration is not very sensitive to
284 their presence at sub-annual time scales. This is because long periods of no-flow contribute
285 very little to the local variance of the time series. The presence of no-flow periods does
286 contribute to the signature of annual variability in the flow regimes. Thus, the power
287 spectral representation at sub-annual timescales can loosely be thought of as representing
288 the hydrological and chemical processes manifested during periods of flow.

289 **2.3.2. Wavelet and wavelet coherence analysis**

290 A wavelet power spectrum (denoted as $|Q^W(f, t)|^2$) can be computed by convolving
291 the timeseries with a function known as the ‘mother wavelet’, and taking the modulus of
292 the resulting wavelet coefficients. Unlike a Fourier transform, which transforms the entire
293 timeseries globally, the wavelet transform decomposes the variance of the timeseries into
294 both frequency and time. By varying the width of the mother wavelet, the contribution of

295 different frequencies to the timeseries variance may be computed at all points in time over
 296 multiple frequency scales (referred to as ‘dyads’) [*Torrence and Compo, 1998; Grinsted*
 297 *et al., 2004*]. Edge effects associated with the convolution of a continuous wavelet and a
 298 finite timeseries reduce the confidence in the computed spectrum near the beginning and
 299 end of the timeseries. This reduction in confidence is most significant at long timescales,
 300 resulting in an internal region within which the spectrum is not influenced by the edge
 301 effects. The area beyond that region is called the “cone of influence” (COI), where the
 302 wavelet spectrum is not reliable. The COI has therefore been excluded from this anal-
 303 ysis [*Kumar and Foufoula-Georgiou, 1997; Grinsted et al., 2004*]. The localized wavelet
 304 power spectrum can be converted to a global spectrum by averaging over the temporal
 305 variability (again excluding the COI). Generally the global wavelet power spectrum is
 306 highly comparable (in at least a qualitative sense) to the power spectrum generated by
 307 Fourier analysis, and again represents a variance partitioning by frequency.

308 Because the covariation between power spectra of flow, concentration and load are of
 309 interest, additional techniques are needed to examine correlations between these differ-
 310 ent spectra. Across all scales we examined such correlations with the wavelet coherence
 311 ($R^2(f)$). $R^2(f)$ of timeseries X and Y is defined as *Grinsted et al.* [2004]:

$$R^2(f) = \frac{|S(f^{-1}XY^w(f))^2|}{S(f^{-1}|X^w(f)|^2) \cdot S(f^{-1}|Y^w(f)|^2)} \quad (3)$$

312 where S is a smoothing operator (chosen to have a similar footprint as the mother wavelet,
 313 here we used a Morlet wavelet) and $XY^w(f)$ is the cross wavelet spectrum of timeseries X
 314 and Y . The reader is referred to *Grinsted et al.* [2004] for further discussion. The wavelet
 315 coherence overall may be interpreted analogously to a correlation coefficient (r^2) between

316 X and Y , but in the frequency domain. Again the wavelet coherence can be computed
 317 locally or averaged across time in order to produce a global wavelet coherence (GWC).
 318 Figure 2 (F) and (G) show the full wavelet spectra of flow and nitrate concentration
 319 respectively for tile flow station B_1 , and Figure 2 (H) shows the wavelet coherence for
 320 these two timeseries.

321 2.3.3. Relationships in the Time Domain: Multi-Resolution Analysis

322 A further use of wavelet techniques in timeseries analysis is as a mechanism to filter
 323 the timeseries and isolate contributions at different frequencies. This technique is known
 324 as multi-resolution analysis (MRA). MRA uses the hierarchical structure of the wavelet
 325 transform to isolate contributions to the variance of the full timeseries at individual dyads
 326 (designated level j), providing a timeseries of fluctuations of level j , referred to as the
 327 detailed signature. Mathematically, this is defined as [*Martinez and Amparo Gilabert,*
 328 2009]:

$$D_j(t) = \sum_{k=-\infty}^{\infty} W_{j,k} \Psi_{j,k}(t), \quad (4)$$

329 where $W_{j,k}$ are the wavelet coefficients at dyad j for each time point k , and $\Psi_{j,k}$ repre-
 330 sents the mother wavelet. By filtering the timeseries at each dyad j and retrieving the
 331 detailed component, a reconstructed timeseries that contains only fluctuations of period
 332 j or greater can be computed from the remainder of the timeseries. These reconstructed
 333 timeseries are referred to as the approximation timeseries [*Martinez and Amparo Gilabert,*
 334 2009], and are mathematically defined as:

$$A_j(t) = \sum_{k=-\infty}^{\infty} V_{j,k} \Phi_{j,k}(t) \quad (5)$$

335 where $V_{j,k}$ are the scaling coefficients and $\Phi_{j,k}$ is the father scaling function.

336 By examining the relationships between the approximation timeseries of L and Q we
337 gain detailed insight into the scales of averaging at which a deterministic (linear) $L - Q$
338 relationship explains most of the variation in L and at which L is thus most predictable.
339 In order to avoid spurious relationships within the correlation analysis, the MRA was
340 undertaken using a Haar wavelet, which does not interpolate between different time points.
341 An example of the approximation and detailed timeseries generated from the MRA are
342 provided in Figure 3.

2.4. Analyses undertaken

343 The specific analyses of the LVR dataset undertaken using the techniques above are
344 summarized in Table 2. Fourier spectral analysis was used to examine the scaling proper-
345 ties of the hydrological and biogeochemical signals. Factors affecting chemostatic behavior
346 in $L - Q$ were investigated by: i) examining the ratio of the power spectra of load and
347 discharge; ii) computing the Global wavelet coherence (GWC), and iii) calculating the
348 correlation between the approximated timeseries of L and Q , generated from MRA at
349 inter-annual timescale.

3. Results and discussion

3.1. Fourier spectral analysis of precipitation-normalized discharge

350 The scaling exponents α that describe the power spectra of discharge (normalized by
351 precipitation) in each of the surface, tile flow and river channel stations are presented
352 in Figure 4. The frequencies of the breaks in scale are reported in Table 3. Error bars
353 on each of the points reflect the standard error of the fitted slopes. Two trends emerge

354 strongly: firstly the number of scaling regimes that can be identified in the flow signature
 355 increases from two in the surface flow stations to three regimes in the tile and river-channel
 356 stations. Secondly, the value of the high-frequency scaling exponents also increases from
 357 ~ 0.5 in the surface drains to ~ 1.25 in the tile drains, and ~ 2 in the river stations. The
 358 low-frequency scaling exponents are comparable between all sites and are approximately
 359 zero. This white noise signature is the residual signal from rainfall forcing on the system.
 360 The mid-range and high frequency exponents increase systematically from tile drain to
 361 river channel, indicating increased modification of the flow signature.

362 We hypothesize that the different observed scaling regimes each arise from a different
 363 set of processes. As a further hypothesis, we consider a multiplicative Fourier Domain
 364 representation of the scaling in which the power spectrum can be decomposed into the
 365 contributions from multiple processes (c.f. *Dolgonosov et al.* [2008]):

$$|Q(f)|^2/|P(f)|^2 \approx \frac{1}{f^{\alpha_1 + \beta_1}} \cdot \frac{1}{f^{\alpha_2 + \beta_2}} \cdots \quad (6)$$

366 where α_i and β_i are parameters representing the power spectrum of a process that con-
 367 tributes to the overall $|Q(f)|^2/|P(f)|^2$ spectrum. This simple model of multiple fre-
 368 quency regimes allows us to mathematically link several features of the observed spectra
 369 to underlying scaling regimes. Firstly, at sufficiently low frequencies, Equation 6 approxi-
 370 mates white noise, which can be interpreted as indicating a regime in which all discharge
 371 responses reflect rainfall forcing. Assuming $\beta_1 \gg \beta_2$, the transition from power law scal-
 372 ing to white noise occurs at frequencies where $f^{\alpha_1} \sim \beta_1$. The strictest interpretation is
 373 that these transitions represent the timescales when the flow path of interest stops con-
 374 tributing noticeably to the variance of the timeseries. We can therefore interpret $1/\beta_1$ as

375 an estimate of the duration of the pressure wave generating transport in the flow path of
376 interest at any particular spatial scale. The appearance of white noise scaling at relatively
377 high frequencies / low residence times ($f = 1/12$) in the surface flow stations compared
378 to the tile and rivers ($f = 1/120$) is consistent with this interpretation. Secondly, the
379 relative magnitudes of α_1 and α_2 can be computed by calculating the difference ($\Delta\alpha$) in
380 exponents between different scaling regimes (provided this calculation occurs well away
381 from the breakpoints where mixed terms – e.g. $\beta_2 \cdot \alpha_1$ – contribute strongly to the scaling).

382 $\Delta\alpha$ between the mid and high frequency scaling regimes in both the tile drain and the
383 surface flow were both approximately 0.5. That is, the flow processes in the tile drain
384 reflect the same spectral pattern as in the surface drain at high frequencies, but contain
385 an additional scaling regime which we attribute to the influence of subsurface processes.
386 Because the surface and subsurface drainage networks are comparable in their extent, it
387 is tempting to attribute the similarity in $\Delta\alpha \sim 0.5$ in each flow station primarily to free
388 surface or pipe flow in the surface and subsurface drainage networks. The appearance
389 of the second scaling regime (medium-low frequencies) in the tile drain would then seem
390 to indicate a process with much slower fluctuations which is presumably related to the
391 timescales at which the water table depth, or equivalently, the volume of the available
392 water storage fluctuates. When comparing the low-mid frequency exponents between the
393 tile drain and the river channel we again compute highly comparable $\Delta\alpha$ values ($\sim 0.5-1$),
394 which we interpret as being the signature of water table - driven tile flow discharge on the
395 whole watershed [*van der Velde et al.*, 2009]. This is consistent with the known significance
396 of tile drainage as comprising 90% of streamflow in the LVR [*Algoazany*, 2006]. The large
397 $\Delta\alpha$ values associated with the high frequency river flow regime reflect the much larger area

398 sampled by the river network and the increased storage and travel times in this regime.
399 Thus, R_3 has larger $\Delta\alpha$ than R_5 , consistent with its larger drainage area. With one
400 exception, the identification of an intermediate scaling regime was statistically significant
401 (at a 95% confidence level). In all cases, the correspondence between the observed $\Delta\alpha$
402 values in the different flow regimes remains striking. Consequently, we interpret the
403 spectral signatures observed at each station as reflecting differing degrees of hydrological
404 filtering by the landscape, drainage and river networks.

3.2. Fourier spectral analysis of concentration timeseries

405 The scaling exponents α describing the power spectra of concentration for each of the
406 solutes in the surface, tile flow and river channel stations are presented in Figure 5, and
407 the scale breaks are reported in Table 3.

408 In many respects the trends in the concentration spectra mirror those in the flow spectra,
409 indicating the importance of flowpaths in dictating the concentration dynamics. Again,
410 the lowest exponents arise in the surface drains, where all solutes behave similarly. The
411 influence of subsurface flow is evident in the higher values of α in the tile-flow drains.
412 Similarly to Figure 4, the low-frequency river exponents are well approximated by the
413 tile-flow exponents. The scale breaks in the concentration spectra are also closely aligned
414 with the mid-high frequency scale breaks in the $|Q(f)|^2/|P(f)|^2$ spectra. The greatest
415 difference between the three solutes is a greater α for nitrate in both the tile-flow exponents
416 and the low-frequency river-scale exponents when compared to phosphate and atrazine.
417 We attribute these differences primarily to the different sorptivities of the chemicals.
418 The appearance of phosphate and atrazine in tile drain flow mostly occurs shortly after
419 application, and presumably reflects rapid transport via a network of preferential flow

420 paths in the vadose zone [*Kladivko et al.*, 1999, 2001; *Haws et al.*, 2004, 2005]. Phosphate
421 has the highest sorptivity coefficient of the three chemicals, and its transport is primarily
422 associated with very large flow events (this can be directly verified by consideration of
423 chemograph and hydrograph data, and is consistent with the numerical predictions of
424 *McGrath* [2007] that suggest that the relative proportion of export occurring in fast flow
425 pathways scaled with sorption.). Under these conditions, preferential macropore flow likely
426 contributes a majority of the flow to the tile drain. The very short residence times (usually
427 ~ 1 hr for 1m depth flow to tiles, [*Haws et al.*, 2004, 2005]) associated with macropore
428 flow mean that this flow path has only a weak spectral signature: consequently flow in the
429 tile network again is the dominant term. This accounts for the strong similarities between
430 phosphate spectra in both surface and tile flow. Note that given the flat topography
431 and similar spatial area drained, residence times in overland flow and the tiles are likely
432 to be similar. In contrast, nitrate has longer residence times in both the saturated and
433 unsaturated zones and, as can again be verified from chemograph and hydrograph data,
434 nitrate is exported in almost all flow events. Plainly atrazine has a spectral signature that
435 is intermediate between the two cases, and examination of chemograph and hydrograph
436 data indicates that although atrazine is primarily exported during large flow events, it
437 continues to be mobilized in smaller events where phosphate was largely absent, and
438 consequently exhibits an ‘intermediate’ spectral exponent in the tile flow. It appears,
439 therefore, that the tile flow exponents primarily reflect the relative sorption of the three
440 chemicals. Surprisingly, the effect of reactivity and the shorter half-lives of phosphate
441 and atrazine compared to nitrate in the catchment (see high frequency components of
442 R3 and R5 in Figure 5) do not appear strongly in this signature, again presumably due

443 to the minimal contribution of periods of no export to the variance of the concentration
444 timeseries.

3.3. Fourier spectral analysis of $|L(f)|^2/|Q(f)|^2$ Ratio

445 As discussed in Section 2.3.1, deviations from white noise scaling in the ratio of
446 $|L(f)|^2/|Q(f)|^2$ are indicative of scaling processes that deviate from the chemostatic
447 hypothesis. At long timescales, $|L(f)|^2/|Q(f)|^2$ associated with all hydrological flow
448 paths and all chemical constituents tended towards white noise. However, the smallest
449 timescale at which this white noise regime was encountered varied with the flow path and
450 the solute, as shown in Table 3.

451 All solutes behaved similarly to each other in the surface stations with the
452 $|L(f)|^2/|Q(f)|^2$ spectra approximating white noise at all scales. This suggests that
453 mobilization is the dominant process contributing to export via surface flow paths, and
454 there are not significant variations in the chemical composition of water transported in
455 this path over different timescales. The white noise scaling regimes were similar for all
456 solutes in the tile and river stations, suggesting that alterations to the chemistry occur
457 primarily in the subsurface flow paths. The nitrate $|L(f)|^2/|Q(f)|^2$ ratio was white noise
458 at almost all locations and scales, i.e. nitrate displayed chemostatic behavior everywhere.
459 This reflects two factors: that $K_d \sim 0$ for nitrate, meaning that it is highly mobile; and
460 the presence of a large reservoir of nitrogen (which, based on previous studies is antic-
461 ipated to consist primarily of organic nitrogen [*Goss et al.*, 1993; *Addiscott*, 1996]) and
462 which is not significantly depleted by the ongoing efflux. Both atrazine and phosphate
463 spectra showed distinct power-law scaling regimes indicating timescales over which bio-
464 geochemical processes strongly modulate the observed transport behavior and prevent the

465 emergence of chemostatic regimes. The timescales on which the power law scaling regime
466 for atrazine transitioned to white noise (approximately 60 days) corresponds closely to
467 the degradation timescale of atrazine. This scaling regime may therefore reflect the rate
468 of disappearance of atrazine from the system. Reaction timescales are much more diffi-
469 cult to define for P because of its complex biogeochemistry [Reddy *et al.*, 2005], but the
470 spectral signature suggests that an ‘effective’ reaction timescale, also on the order of 60
471 days, could be hypothesized to describe the immobilization of P in the LVR. An alter-
472 native interpretation, however, is that the common 60-day timescale in both cases reflect
473 the typical timescales of crop growth and uptake. Evidently, separating biological uptake
474 from geochemical processes remains difficult on the basis of stream concentrations alone.
475 Overall, however, it appeared that the most mobile of the constituents, nitrate displayed
476 the most chemostatic behavior.

3.4. Wavelet coherence analysis of L-Q and C-Q

477 Wavelet coherence can be interpreted analogously to a Pearson’s Correlation Coefficient
478 in the frequency domain (see detail in section 2.3.2 and Figure 7), and can be used to
479 identify if processes occurring at a particular timescale generate the same responses in
480 two different signals. Loosely this can be interpreted as the strength of coupling between
481 two different signals over a range of frequencies. Figure 6 gives examples of the wavelet
482 coherence of flow and nitrate concentration for each of the three types of sites, showing a
483 progressive decoupling of flow and concentration from surface drains to tile drains and the
484 river station. Global wavelet coherence (GWC) plots for the exported load and concen-
485 tration of each solute at each scale are presented in Figure 7. The GWC differs with the
486 flow path and with solute type. In the surface flow stations a strong coupling between dis-

487 charge and concentration and discharge and load was found for all solutes. At within-year
488 timescales, tile flow stations showed a lower degree of coupling than the surface stations,
489 but a stronger coupling than in the river channel. This was particularly exaggerated in
490 the concentration - discharge GWC. However, at annual or longer scales, the coupling
491 between load-discharge and concentration-discharge in the river stations increased.

492 The wavelet coherence plots suggest several features of the coupling between flow and
493 biogeochemistry. However, caution is needed when interpreting this coupling between
494 two timeseries, because the wavelet coherence reflects the timing of fluctuations, but not
495 necessarily their magnitude. Consequently, we see a significant coherence between flow
496 and load at all timescales (Figure 7A), because load is a function of flow. Conversely, high
497 coherence between discharge and concentration only emerges at annual timescales (Figure
498 7B), reflecting the dominant annual anthropogenic forcing associated with fertilizer and
499 pesticide application. The fact that the strongest phosphate-flow coupling arose not at
500 the annual but longer timescales is reflected in the recorded fertilization dates for the
501 LVR. Phosphate has more irregular fertilizing timing compared to nitrate and atrazine,
502 both of which have regular annual cycles of application.

3.5. Multi-resolution analysis of L-Q

503 We examined patterns in the r^2 values for a linear regression between L and Q evaluated
504 on each dyadic level of the approximation timeseries generated from the MRA (c.f. Figure
505 3). Across the majority of the sites and chemical species we found that the r^2 peaked at
506 the dyadic level associated with variation on 128-255 day timescales. The approximation
507 timeseries at this level preserves variation on seasonal timescales and greater (timescales
508 which resolve variations in chemical application, and the annual cropping cycles), but

509 smooths over within-season variation. The r^2 values generated at this smoothing level
510 for the linear $L - Q$ regression across all chemical species and sites are presented in
511 Figure 8. The surface drainage r^2 values were highly variable, while the tile flow and
512 river channel sites were more consistent both across sites and between the river and tile
513 stations. nitrate displayed high r^2 values at all stations, while the r^2 values of $L - Q$ for
514 atrazine and phosphate declined from surface flow stations to tile and river stations.

515 The highly variable $L - Q$ r^2 in the three surface drains is difficult to explain and
516 presumably reflects site-to-site differences (e.g. in local topography, drain design, crops,
517 agricultural practices and resulting availability of the phosphate sources). The minimal
518 differences in the r^2 behavior at tile and river stations appears to be consistent with the
519 similarities in the scaling behavior of C and Q in tile and river stations at low frequencies
520 as shown in Figures 4 and 5. The primary deviations in transport processes between
521 these systems were associated with high-frequencies, which are essentially removed by
522 the wavelet filtering. The large declines in phosphate and atrazine $L - Q$ r^2 in tile and
523 river stations versus surface stations reflect the importance of subsurface biogeochemical
524 processes in altering the availability and mobility of these chemicals, consistent with the
525 observations in Table 3. These results indicate that there is a distinct difference in the
526 degree of chemostatic response observed for the three chemical species at the inter-annual
527 scale, with nitrate being the most ‘chemostatic’, and atrazine the least.

4. Summary and conclusions

528 This study was motivated by three key questions: 1) How do concentration and flow
529 scale in the frequency domain (as metrics of filtering)? 2) Does the observed scaling
530 behavior ‘fingerprint’ different reactive transport processes? and 3) On what spatial and

531 temporal scales are chemostatic responses observed for the three chemicals considered?
532 We can now answer these questions explicitly on the basis of the analysis above. It must
533 be recognized, however, that process diagnosis on the basis of timeseries analysis alone
534 is not definitive, but rather forms the basis for a conceptual model of solute filtering in
535 the catchment. More explicit verification of the interpretations offered below is necessary,
536 and is discussed as part of the Future Work section. However, for clarity, an illustration
537 of the conceptual model of hydrological and biogeochemical filtering in the catchment
538 that emerges from the frequency-based analysis is presented in Figure 9 and is referred to
539 throughout this discussion.

4.1. How do concentration and flow scale?

540 Concentration and flow scaling regimes showed strong parallels. The major trend in
541 the scaling exponents for both solute concentration and the normalized flow (see Figures
542 4 and 5), was the increase across hydrologic flow paths and spatial scales from surface
543 drain to the tile flow stations, with further increases in the river stations. This trend
544 can be broadly linked to increased catchment residence times at each scale, and process
545 relationships to the scaling regimes may be inferred by considering the breaks in scaling
546 and the response of different solutes. Specifically, it appears that the highest frequency
547 scaling regimes in R3 and R5 relate to tile or surface flow in the networks: either the
548 surface drain network (Figure 9, filter *i*), the tile drain network (filter *iii*), or the river
549 network (filter *v*). The similarities in discharge $\Delta\alpha$ associated with the low-frequency -
550 mid-frequency scaling regimes for Q in the tile stations and the river channels, along with
551 the absence of an intermediate scaling regime in the surface flow case strongly suggest
552 that this frequency range is dominated by slower modulations of the water table and

553 consequently the storage capacity in the soil (Figure 9, filters *ii* and *iv*). The clear
554 emergence of three scaling regimes in the stream discharge suggests that timescales of
555 transport in a diversity of runoff pathways in agricultural catchments may be inferred on
556 the basis of flow data from the streams alone. Filtering flow and concentration timeseries
557 at scales that correspond to these different regimes may even allow estimates of the mass
558 contribution associated with these distinct flow paths to be made on the basis of in-stream
559 concentrations, offering complementary approach to requiring explicit observation of all
560 contributions in the catchment (c.f. *Rozemeijer et al.* [2010a]).

4.2. Can we identify reactive transport processes?

561 By linking the scaling regimes of discharge and concentration, we argue that signa-
562 tures of reactive transport processes and pathways can be inferred. Although phosphate,
563 atrazine and nitrate are all exported by the tile drains, much larger scaling exponents
564 are associated with nitrate compared to phosphate or atrazine in the tile drains and the
565 low-frequency regime of the river stations. We interpret this observation by suggesting
566 that these scaling regimes are associated with primarily a vadose zone-macropore flow
567 path for phosphate and atrazine (Figure 9, filter *ii*), but a vadose zone-saturated zone
568 flow path for nitrate (Figure 9, filter *iv*). This is consistent with the higher application
569 rates of nitrate compared to atrazine and phosphate, resulting in larger concentrations and
570 residence times of nitrate in the subsurface, and with the importance of surface chemistry
571 in retaining P and atrazine in the soil matrix and thus favoring transport in macropores
572 [*Haws et al.*, 2004]. Thus, the different scaling behavior of nitrate in the tile and river
573 stations appears to act as a fingerprint both of the location of mobile stores of the different
574 chemicals (soil surface / vadose zone dominated for phosphate and atrazine, vadose zone

575 / water-table dominated for nitrate); and of the different transport pathways that control
576 mobilization of the solutes (Figure 9, filters *ii* and *iv*)).

577 This interpretation also appears consistent with the analysis of $|L(f)|^2/|Q(f)|^2$ for
578 the different solutes. If long-term reservoirs of nitrate are present in the subsurface then
579 its export may be primarily driven by transport processes, so that the approximation of
580 $|L(f)|^2/|Q(f)|^2$ as white noise at all scales is reasonable. In contrast, the export behavior
581 of atrazine and phosphate is modified by the timescales of removal (geochemically or due
582 to plant uptake), and also potentially by dilution processes (e.g. between macropore flow
583 and water table contributions) in the tile drains. The emergence of scaling behavior in
584 $|L(f)|^2/|Q(f)|^2$, may reflect biological, chemical and mixing processes. Note, however,
585 that the absence of deviations from white noise scaling in the $|L(f)|^2/|Q(f)|^2$ ratio does
586 not imply the absence of removal processes, but merely that these removal processes do
587 not alter the variance partitioning in the concentration signal. To resolve this ambiguity,
588 spectral analysis could be complemented by mass balance approaches to offer deeper
589 insight into reactive transport.

590 The concentration scaling regimes in the river channel appeared invariant with scale
591 for phosphate and atrazine, but were scale dependent for nitrate. This suggests that
592 timescales of removal of phosphate and atrazine are either much larger or much smaller
593 than the residence times R_5 (the upper-catchment river station). Indeed, atrazine removal
594 rates from surface waters are almost negligible [*Capel and Larson, 2001*]. Conversely, the
595 higher $\Delta\alpha$ for nitrate at R_5 (~ 0.75) than R_3 (~ 1.25) suggests that in-channel processing
596 or removal became more significant with increasing scale, potentially reflecting the greater
597 residence time in the system.

4.3. When does chemostatic behavior occur?

598 Chemostatic behavior was most prevalent in the Little Vermilion River Watershed on
599 seasonal to annual timescales, and for chemicals where the rate of removal from transport
600 was comparable or slower than the timescales of chemical renewal. The former condition
601 reflects the importance of annual or inter-annual applications of chemicals in controlling
602 the mass of solute available for export (and was reflected by e.g. the strong coherence
603 in the $C - Q$ and $L - Q$ wavelet coherence at annual timescales). The latter condition
604 allows a pseudo-steady concentration of mobile solute to persist in subsurface reservoirs.
605 Export from the subsurface is sensitive to the availability of water to drive transport:
606 thus loads respond strongly to variation in flow. In the Little Vermilion River Watershed,
607 chemostatic behavior arises from the combination of human modification of hydrological
608 flow paths and human amendment of the biogeochemical regime through regular addition
609 of agrochemicals. The addition of fertilizers/pesticides is large in comparison to the
610 capacity of natural biogeochemical processes to cycle and remove these chemicals from
611 the system. This leads to a minimal influence of biogeochemical cycling on the resulting
612 chemical export in comparison to anthropogenic forcing. This allows for accumulation of
613 nutrient stores in soils which is the manifestation of intensive management over the past
614 several decades. Similarly, the modification of the hydrology reduces both the mean and
615 the variance of residence times in the catchment, preventing hydrological complexity from
616 obscuring the chemostatic signals.

4.4. Implications for environmental management

617 Limited in-stream processing and resulting emergence of near linear load-flow relation-
618 ships is well established at large scales in the Mississippi-Missouri River Basin [*Basu et al.*,

619 2010a]. The analysis presented here demonstrates that such behavior is also characteris-
620 tic of export at the smallest scales (tile and surface drainage areas) contributing flow and
621 chemicals to the river systems. That is, anthropogenic impacts appear to override natural
622 biogeochemical processing at all spatial scales in the basin.

4.5. Broader implications and future work

623 The simplicity of hydrological pathways in the Little Vermilion River Watershed allowed
624 us to inferentially link the observed discharge, load and concentration scaling regimes to
625 hydrological and chemical processes. There may be potential to use similar observa-
626 tions of scaling regimes to learn about runoff pathways in more complex catchments,
627 if the observed scaling regimes can be unambiguously linked to different runoff genera-
628 tion mechanisms. In larger, more complex catchment systems, similar scaling regimes in
629 streamflow are known to arise [*Milly and Wetherald, 2002; Dolgonosov et al., 2008*]. Pre-
630 viously authors have tended to relate the observed scaling regimes to bulk representations
631 of catchment reservoir models [*Milly and Wetherald, 2002*], attributing the break in scale
632 at weekly - monthly timescales to spatial variation in rainfall [*Dolgonosov et al., 2008*].
633 This study has highlighted the potential for the different scaling regimes to reflect runoff
634 regimes associated primarily with fast flow generation processes, and with the slower mod-
635 ulations of baseflow by changes in water table depth [*Zhang and Schilling, 2004*]. It is
636 intriguing to speculate that, at least in these agricultural settings, the breaks in scaling
637 could be used to develop appropriate windows to use for hydrograph separation. *Wörman*
638 *et al.* [2010] have shown that systematic changes in the spectral properties of streamflow
639 over time may be links to human impacts such as stream damming and land use change,

640 suggesting that scaling exponents may also have a role as indicators of hydrological and
641 catchment-scale change.

642 The conceptual model developed from inference based on the frequency-domain analysis
643 here is not definitive, and further verification is needed. One approach for such verification
644 is to develop process-based models of hydrological and biogeochemical response in tile-
645 drained agricultural catchments that could represent the different processes associated
646 with nitrate, phosphate and atrazine mobilization. In particular, spatial and temporal
647 intermittency in the application of pesticides and fertilizers between different farms in the
648 catchment leads to spatio-temporal variability in the forcing on the catchment. The impli-
649 cations of this variation for the emerging spectral signatures of concentration are not well
650 defined and could not be definitively isolated within the Little Vermillion River Watershed
651 dataset. The precise translation of this variability into the properties of the power-spectra
652 of export requires further investigation to assist in the robust interpretation of concentra-
653 tion data at large spatial scales. Convergence of the patterns of export predicted by such
654 process-based models to observations in the LVR would provide additional verification
655 of the conceptual model. The Fourier and wavelet spectra and the multi-resolution sig-
656 natures of hydrology and biogeochemistry in the catchment provide excellent targets for
657 model validation. Similarly, frequency-based tools in either the Fourier or wavelet domain
658 offer alternative approaches for model diagnostics, which complement diagnostics based
659 purely on matching timeseries [*Siqueira et al.*, 2006; *Mahecha et al.*, 2010; *Schaefli and*
660 *Zehe*, 2009]. Time domain validation is biased towards identifying the processes which
661 contribute most of the variance over the length of the simulation. By contrast, frequency

662 domain validation identifies scales where a model performs poorly, potentially helping to
663 identify missing processes or knowledge gaps.

664 Conceptualizing catchments as filters originally offered new perspectives on timeseries
665 analysis and the propagation of rainfall into surface and subsurface runoff. It appears
666 that at least in simple systems it is possible to link the characteristics of the resulting
667 scaling regimes to identifiable physical processes that take place within the catchments,
668 allowing the filter concept to be linked to mechanistic understanding of rainfall-runoff re-
669 sponse. More fundamentally, however, the filter concept appears to have new applicability
670 as catchments are increasingly visualized as complex systems in which biogeochemical and
671 ecological processes respond to rainfall and streamflow drivers. As high resolution concen-
672 tration and flow datasets become available from a wider range of sites, the biogeochemical
673 aspects of this filtering can be explored further. Expanding the filter concept of catch-
674 ments to ecological processes, with their many complex drivers, remains an important
675 frontier for future work.

676 **Acknowledgments.** This study was conducted as part of the NSF-funded Hydrologic
677 Synthesis project: *Water Cycle Dynamics in a Changing Environment: Advancing Hydro-*
678 *logic Science through Synthesis* (NSF Grant EAR-0636043, M. Sivapalan, PI). We thank
679 Anders Wörman for constructive comments on the manuscript.

References

680 Addiscott, T. (1996), Fertilizers and nitrate leaching, in *Agricultural Chemicals and the*
681 *Environment, Issues in Environmental Science and Technology*, vol. 5, pp. 1–26, Royal
682 Society of Chemistry, Cambridge.

- 683 Algoazany, A. (2006), Long-term effects of agricultural chemicals and management prac-
684 tices on water quality in a subsurface drained watershed, Ph.D. thesis, University of
685 Illinois at Urbana Champaign.
- 686 Basu, N. B., P. S. C. Rao, E. H. Winzeler, S. Kumar, P. R. Owens, and V. Mer-
687 wade (2010a), Identification of dominant controls on hydrologic responses in engi-
688 neered watersheds: 1. Hydrograph prediction, *Water Resources Research*, doi:10.1029/
689 2009WR007803.
- 690 Basu, N. B., G. Destouni, J. W. Jawitz, S. E. Thompson, N. Loukinova, A. Darracq,
691 S. Zanardo, M. Yaeger, M. Sivapalan, A. Rinaldo, and P. S. C. Rao (2010b), Nutrient
692 loads exported from managed catchments reveal emergent biogeochemical stationarity,
693 *Geophysical Research Letters*, 37(L23404), doi:10.1029/2010GL045168.
- 694 Blann, K., J. Anderson, G. Sands, and B. Vondracek (2009), Effect of agricultural drainage
695 on aquatic ecosystems: A review, *Critical Reviews in Environmental Science and Tech-*
696 *nology*, 39(11), 909–1001.
- 697 Borsuk, M., C. Stow, and K. Reckhow (2004), Confounding effect of flow on estuarine
698 response to nitrogen loading, *Journal of Environmental Engineering - ASCE*, 130(6),
699 605–614, doi:{10.1061/(ASCE)0733-9372}.
- 700 Botter, G., E. Bertuzzo, and A. Rinaldo (2010), Transport in the hydrologic response:
701 Travel time distributions, soil moisture dynamics, and the old water paradox, *Water*
702 *Resources Research*, 46, doi:0.1029/2009WR008371.
- 703 Brusseau, M. L., and P. S. C. Rao (1989), Sorption nonideality during organic contaminant
704 transport in porous media, *CRC Critical Reviews in Environmental Science*, 19(1), 33–
705 99.

- 706 Capel, P., and S. Larson (2001), Effect of scale on the behavior of atrazine in surface
707 waters, *Environmental Science & Technology*, *35*(4), 648–657, doi:{10.1021/es001220f}.
- 708 Cardenas, M. B. (2008), Surface water-groundwater interface geomorphology leads
709 to scaling of residence times, *Geophysical Research Letters*, *35*(8), doi:{10.1029/
710 2008GL033753}.
- 711 Dolgonosov, B., K. Korchagin, and N. Kirpichnikova (2008), Modeling of annual oscilla-
712 tions and 1/f-noise of daily river discharges, *Journal of Hydrology*, *357*(3-4), 174–187,
713 doi:10.1016/j.jhydrol.2008.04.023.
- 714 Evans, R. O., and N. R. Fausey (1999), Effects of inadequate drainage on crop growth
715 and yield, in *Agricultural Drainage*, vol. 1, pp. 13–54, American Society of Agronomy,
716 Madison, Wisconsin.
- 717 Feng, X., J. W. Kirchner, and C. Neal (2004a), Measuring catchment-scale chemical
718 retardation using spectral analysis of reactive and passive chemical tracer time series,
719 *Journal of Hydrology*, *292*(1-4), 296 – 307, doi:10.1016/j.jhydrol.2004.01.012.
- 720 Feng, X., J. W. Kirchner, and C. Neal (2004b), Spectral analysis of chemical time se-
721 ries from long-term catchment monitoring studies: Hydrochemical insights and data
722 requirements, *Water, Air, & Soil Pollution: Focus*, *4*(2-3), 221–235, doi:10.1023/B:
723 WAFO.0000028356.24722.b1.
- 724 Fraedrich, K., and C. Larnder (1993), Scaling regimes of composite rainfall time series,
725 *Tellus A*, *45*, 289–298.
- 726 Godsey, S., J. Kirchner, and D. Clow (2009), Concentration-discharge relationships reflect
727 chemostatic characteristics of US catchments, *Hydrological Processes*, *23*(13), 1844–
728 1864.

- 729 Godsey, S. E., W. Aas, T. A. Clair, H. A. de Wit, I. J. Fernandez, J. S. Kahl, I. A.
730 Malcolm, C. Neal, M. Neal, S. J. Nelson, S. A. Norton, M. C. Palucis, B. L. Skjelkvle,
731 C. Soulsby, D. Tetzlaff, and J. W. Kirchner (2010), Generality of fractal $1/f$ scaling in
732 catchment tracer time series, and its implications for catchment travel time distribu-
733 tions, *Hydrological Processes*, *24*(12), doi:10.1002/hyp.7677.
- 734 Goss, M., K. Howse, P. Lane, D. Christian, and G. Harris (1993), Losses of nitrate -
735 nitrogen in water draining from under autumn sown crops established by direct drilling
736 or moldboard plowing, *Journal of Soil Science*, *44*(1), 35–48.
- 737 Grinsted, A., S. Jevrejeva, and J. Moore (2004), Application of the cross-wavelet transform
738 and wavelet coherence to geophysical time series, *Nonlinear Processes in Geophysics*,
739 *11*, 561–566, doi:10.5194/npg-11-561-2004.
- 740 Harris, D., A. Seed, M. Menabde, and G. Austin (1997), Factors affecting multiscaling
741 analysis of rainfall time series, *Nonlinear Processes in Geophysics*, *4*, 137–156.
- 742 Haws, N. W., B. S. Das, and P. S. C. Rao (2004), Dual-domain solute transfer and trans-
743 port processes: evaluation in batch and transport experiments, *Journal of Contaminant*
744 *Hydrology*, *75*(3-4), 257–280, doi:{10.1016/j.jconhyd.2004.07.001}.
- 745 Haws, N. W., P. S. C. Rao, J. Simunek, and I. C. Poyer (2005), Single-porosity and
746 dual-porosity modeling of water flow and solute transport in subsurface-drained fields
747 using effective field-scale parameters, *Journal of Hhydrology*, *313*(3-4), 257–273, doi:
748 {10.1016/j.jhydrol.2005.03.035}.
- 749 Katul, G. G., A. Porporato, E. Daly, A. C. Oishi, H.-S. Kim, P. C. Stoy, J.-Y. Juang,
750 and M. B. Siqueira (2007), On the spectrum of soil moisture from hourly to interannual
751 scales, *Water Resources Research*, *43*(5), doi:{10.1029/2006WR005356}.

- 752 Kirchner, J., X. Feng, and C. Neal (2000), Fractal stream chemistry and its implications
753 for contaminant transport, *Nature*, *403*(6769), 524–527.
- 754 Kirchner, J., X. Feng, and C. Neal (2001), Catchment-scale advection and dispersion as
755 a mechanism for fractal scaling in stream tracer concentrations, *Journal of Hydrology*,
756 *254*(1-4), 82–101.
- 757 Kirchner, J., X. Feng, C. Neal, and A. Robson (2004), The fine structure of water-quality
758 dynamics: the (high-frequency) wave of the future, *Hydrological Processes*, *18*(7), 1353–
759 1359, doi:{10.1002/hyp.5537}.
- 760 Kirchner, J. W. (2009), Catchments as simple dynamical systems: Catchment charac-
761 terization, rainfall-runoff modeling, and doing hydrology backward, *Water Resources*
762 *Research*, *45*(doi:10.1029/2008WR006912).
- 763 Kladivko, E., L. C. Brown, and J. L. Baker (2001), Pesticide transport to subsurface tile
764 drains in humid regions of north america, *Critical Reviews in Environmental Science*
765 *and Technology*, *31*, 1–62.
- 766 Kladivko, E. J., J. Grochulska, R. F. Turco, G. Van Scoyoc, and J. D. Eigel (1999),
767 Pesticide and nitrate transport into subsurface tile drains of different spacing, *Journal*
768 *of Environmental Quality*, *28*, 997–1004.
- 769 Kumar, P., and E. Foufoula-Georgiou (1997), Wavelet analysis for geophysical applica-
770 tions, *Reviews in Geophysics*, *35*(4), 385–412.
- 771 Li, Z., and Y.-K. Zhang (2007), Quantifying fractal dynamics of groundwater systems
772 with detrended fluctuation analysis, *Journal of Hydrology*, *336*(1-2), 139–146, doi:{10.
773 1016/j.jhydrol.2006.12.017}.

774 Machesky, M., T. Holm, and J. Slowikowski (2010), Phosphorus speciation in stream
775 bed sediments from an agricultural watershed: Solid-phase associations and sorption
776 behavior, *Aquatic Geochemistry*, *16*, 639–662, 10.1007/s10498-010-9103-2.

777 Mahecha, M., M. Reichstein, M. Jung, S. Seneviratne, S. Zaehle, C. Beer, M. Braakhekke,
778 N. Carvalhais, H. Lange, G. Le-Maire, and E. Moors (2010), Comparing observa-
779 tions and process based simulations of biosphere-atmosphere exchanges on multi-
780 ple timescales, *Journal of Geophysical Research - Biogeosciences*, *115*(G02003), doi:
781 10.1029/2009JG001016.

782 Majone, B., A. Bellin, and A. Borsato (2004), Runoff generation and contaminant trans-
783 port in karst catchments, *Journal of Hydrology*, *294*(176-195), doi:10.1016/j.jhydrol.
784 2003.11.042.

785 Majone, B., A. Bertagnoli, and A. Bellin (2010), A non-linear runoff generation model in
786 small alpine catchments, *Journal of Hydrology*, *385*(1-4), doi:10.1016/j.jhydrol.2003.11.
787 042.

788 Martinez, B., and M. Amparo Gilabert (2009), Vegetation dynamics from NDVI time
789 series analysis using the wavelet transform, *Remote Sensing of the Environment*, *113*(9),
790 1823–1842, doi:{10.1016/j.rse.2009.04.016}.

791 Matsoukas, C., S. Islam, and I. Rodriguez-Iturbe (2000), Detrended fluctuation analysis
792 of rainfall and streamflow time series, *Journal of Geophysical Research - Atmospheres*,
793 *105*(D23), 29,165–29,172.

794 McGrath, G. (2007), An exploration of the rainfall controls on pesticide transport via fast
795 flow pathways, Ph.D. thesis, School of Earth and Geographical Sciences, University of
796 Western Australia, Perth, Australia.

- 797 McLaughlin, A., and P. Mineau (1995), The impact of agricultural practices on biodiver-
798 sity, *Agriculture, Ecosystems and Environment*, 55(3), 201–212.
- 799 Meng, H., J. Salas, T. Green, and L. Ahuja (2006), Scaling analysis of space-time in-
800 filtration based on the universal multifractal model, *Journal of Hydrology*, 322(1-4),
801 220–235, doi:{10.1016/j.jhydrol.2005.03.016}.
- 802 Milly, P. C. D., and R. T. Wetherald (2002), Macroscale water fluxes 3. Effects of land
803 processes on variability of monthly river discharge, *Water Resources Research*, 38(11),
804 doi:10.1029/2001WR000761.
- 805 Mitchell, J., G. McIsaac, S. Walker, and M. Hirschi (2000), Nitrate in river and subsurface
806 drainage flows from an east central Illinois watershed, *Transactions of the ASAE*, 43(2),
807 337–342.
- 808 Phillips, B., B. Anderson, J. Hunt, S. Huntley, R. Tjeerdema, N. Kapellas, and K. Worces-
809 ter (2006), Soil-phase sediment toxicity identification evaluation in an agricultural
810 stream, *Environmental Toxicology and Chemistry*, 25(6), 1671–1676.
- 811 Rabalais, N., R. Turner, and W. Wiseman (2002), Gulf of Mexico hypoxia, aka “The Dead
812 Zone”, *Annual Review of Ecology and Systematics*, 33, 235–263, doi:10.1146/annurev.
813 ecolsys.33.010802.150513.
- 814 Reddy, K. R., R. G. Wetzel, and R. Kadlec (2005), Biogeochemistry of phosphorus in
815 wetlands, in *Phosphorus: Agriculture and the Environment*, edited by J. T. Sims and
816 A. N. Sharpley, pp. 263–316, Soil Science Society of America.
- 817 Rozemeijer, J. C., Y. van der Velde, R. G. McLaren, F. C. van Geer, H. P. Broers, and
818 M. F. P. Bierkens (2010a), Integrated modeling of groundwater-surface water interac-
819 tions in a tile-drained agricultural field: The importance of directly measured flow route

- 820 contributions, *Water Resources Research*, *46*(W11537), doi:10.1029/2010WR009155.
- 821 Rozemeijer, J. C., Y. van der Velde, F. C. van Geer, G. De Rooij, P. J. J. F. Torfs, and
822 H. P. Broers (2010b), Improving load estimates for NO₃ and P in surface waters by
823 characterizing the concentration response to rainfall events, *Environmental Science and*
824 *Technology*, *44*(16), 6305–6312.
- 825 Sauquet, E., M.-H. Ramos, L. Chapel, and P. Bernardara (2008), Streamflow scaling
826 properties: investigating characteristic scales from different statistical approaches, *Hy-*
827 *drological Processes*, *22*(17), 3462–3475, doi:{10.1002/hyp.6952}.
- 828 Schaeffli, B., and E. Zehe (2009), Hydrological model performance and parameter estima-
829 tion in the wavelet domain, *Hydrology and Earth Systems Science*, *13*, 1921–1936.
- 830 Schertzer, D., P. Bernardara, A. Biaou, I. Tchiguirinskaia, M. Lang, E. Sauquet, H. Bend-
831 joudi, P. Hubert, S. Lovejoy, and J. M. Veysseire (2006), Extremes and multifractals in
832 hydrology: results, validations and prospects, *Houille Blanche - Revue Internationale de*
833 *l'Eau*, *5*, 112–119, doi:{10.1051/lhb:2006095}.
- 834 Schilling, K., and M. Helmers (2008), Effect of subsurface drainage tiles on streamflow in
835 iowa agricultural watersheds: Exploratory hydrograph analysis, *Hydrological Processes*,
836 *22*, 4497 – 4506.
- 837 Siqueira, M., G. Katul, D. Sampson, P. Stoy, J.-Y. Juang, H. McCarthy, and R. Oren
838 (2006), Multiscale model intercomparisons of CO₂ and H₂O exchange rates in a ma-
839 turing Southeastern US pine forest, *Global Change Biology*, *12*, doi:10.1111/j.1365-
840 2486.2006.01,158.x.
- 841 Tessier, Y., S. Lovejoy, P. Hubert, D. Schertzer, and S. Pecknold (1996), Multifractal
842 analysis and modeling of rainfall and river flows and scaling, causal transfer functions,

- 843 *Journal of Geophysical Research - Atmospheres*, 101(D21), 26,427–26,440.
- 844 Torrence, C., and G. Compo (1998), A practical guide to wavelet analysis, *Bulletin of the*
845 *American Meteorological Society*, 79(1), 61–78.
- 846 van der Velde, Y., G. G. de Rooj, and P. J. J. F. Trofs (2009), Catchment-scale non-
847 linear groundwater-surface water interactions in densely drained lowland catchments,
848 *Hydrological and Earth Systems Science*, 13, 1867–1885.
- 849 Wauchope, R. D., T. M. Buttler, A. G. Hornsby, P. W. M. Augustijn-Beckers, and
850 J. P. Burt (1992), The SCS/ARS/CES pesticide properties database for environmental
851 decision-making, in *Reviews of Environmental Contamination and Toxicology*, vol. 123,
852 edited by G. Ware, Springer Verlag, New York.
- 853 Wörman, A., G. Lindstrom, A. Akesson, and J. Riml (2010), Drifting runoff periodicity
854 during the 20th century due to changing surface water volume, *Hydrological Processes*,
855 doi:{10.1002/hyp.7810}.
- 856 Zhang, Y., and K. Schilling (2004), Temporal scaling of hydraulic head and river base
857 flow and its implication for groundwater recharge, *Water Resources Research*, 40(3),
858 doi:{10.1029/2003WR002094}.
- 859 Zhang, Y., and K. Schilling (2005), Temporal variations and scaling of streamflow and
860 baseflow and their nitrate-nitrogen concentrations and loads, *Advances in Water Re-*
861 *sources*, 28(7), 701–710, doi:{10.1016/j.adwatres.2004.12.014}.
- 862 Zhou, X., N. Persaud, H. Wang, and H. Lin (2006), Multifractal scaling of daily runoff time
863 series in agricultural watersheds, *Journal of the American Water Resources Association*,
864 42(6), 1659–1670.

Table 1. Monitoring stations within the Little Vermilion Watershed that will be used in this study. Q thresh indicates the minimum flow at which high frequency monitoring was initiated.

Site	Station	Flow Type	Drainage Area (m ²)	Record Coverage	Q thresh. m ³ /s
A	A1	Subsurface (tile)	4.9×10^4	11/19/1991 – 12/31/2000	10^{-4} m ³ /s
	A2	Surface	6.0×10^4	1/20/1993 – 12/31/2000	10^{-4} m ³ /s
B	B1	Subsurface (tile)	3.3×10^4	11/20/1991 – 12/31/2000	10^{-4} m ³ /s
	B2	Surface	3.0×10^4	07/24/1993 – 12/31/2000	10^{-4} m ³ /s
C	C1	Subsurface (tile)	6.8×10^4	11/07/1992 – 12/31/2000	10^{-4} m ³ /s
	C2	Surface	1.5×10^4	11/17/1993 – 12/31/2000	10^{-4} m ³ /s
R3	R3	River	1.9×10^8	07/12/1993 – 12/31/2000	10^{-2} m ³ /s
R5	R5	River	6.9×10^7	08/14/1992 – 12/31/2000	10^{-2} m ³ /s

Table 2. Analyses undertaken to explore $L - Q$ and $C - Q$ behavior

Analysis	Purpose	Figure Reference
C and Q Dynamics		
Scaling Analysis	Scaling regimes	Fig. 5
Global Wavelet Coherence	Timescales where C-Q Coupling maximized	Fig. 6 & 7
L and Q Dynamics		
Scaling Analysis	Scaling regimes	Fig. 2 & 4
Power Spectral Ratios	Timescales of non-chemostatic processes	Tab. 3
Global Wavelet Coherence	Timescales that maximize predictability	Fig. 2 & 7
MRA Approximation Timeseries	Timescales that maximize predictability	Fig. 3 & 8
Correlative Analysis		

Table 3. Frequencies of break points for Q/P and C , and lowest frequency where $|L(f)|^2/|Q(f)|^2$ is well approximated by white noise. White noise scaling persists from the identified frequency to inter-annual scale ($f = 1/1024$). Variation between replicates of each sampling type was low. Where there was disagreement between sites, the lowest frequency at which white noise commenced is presented. Units of f are day^{-1} , and Atraz indicates atrazine.

Flow path	Q/P scale breaks (f)		Solute	L/Q white noise (f)	C scale breaks (f)
	low-mid	mid-high			low-high
Surface-flow	-	1/12	NO ₃ ¹⁻	1/2	-
			PO ₄ ³⁻	1/2	-
			Atraz	1/2	-
Tile-flow	1/120	1/12	NO ₃ ¹⁻	1/2	-
			PO ₄ ³⁻	1/64	-
			Atraz	1/64	-
River-channel	1/120	1/12	NO ₃ ¹⁻	1/2	1/12
			PO ₄ ³⁻	1/64	1/23
			Atraz	1/128	1/12

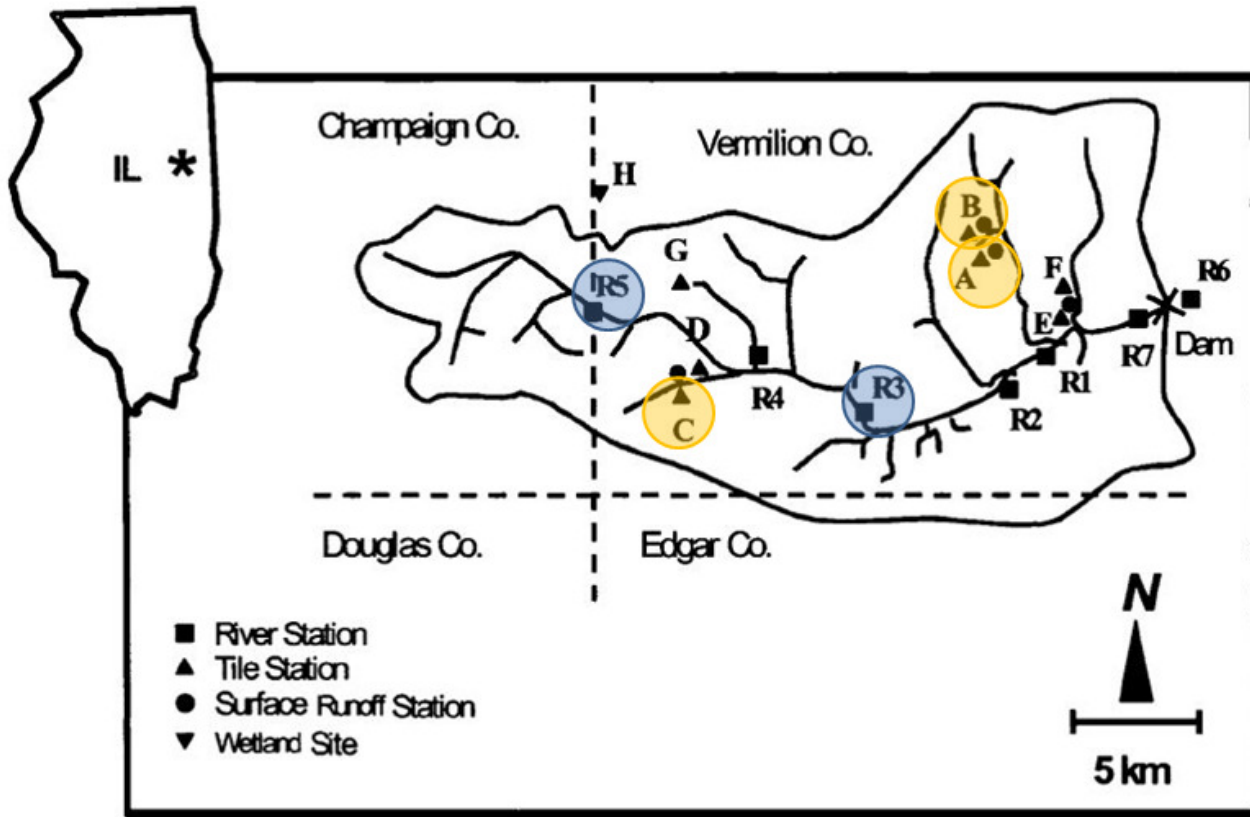


Figure 1. The Little Vermilion River Watershed (LVR), Illinois, USA, ($40^{\circ}06'21.45''N$, $87^{\circ}41'34.12''W$). The focus of the study is on three co-located tile and surface drainage stations (denoted A_1/A_2 , B_1/B_2 and C_1/C_2 , where 1 indicates a subsurface tile drain and 2 indicates a surface drain), and two river gauges (R_3 and R_5).

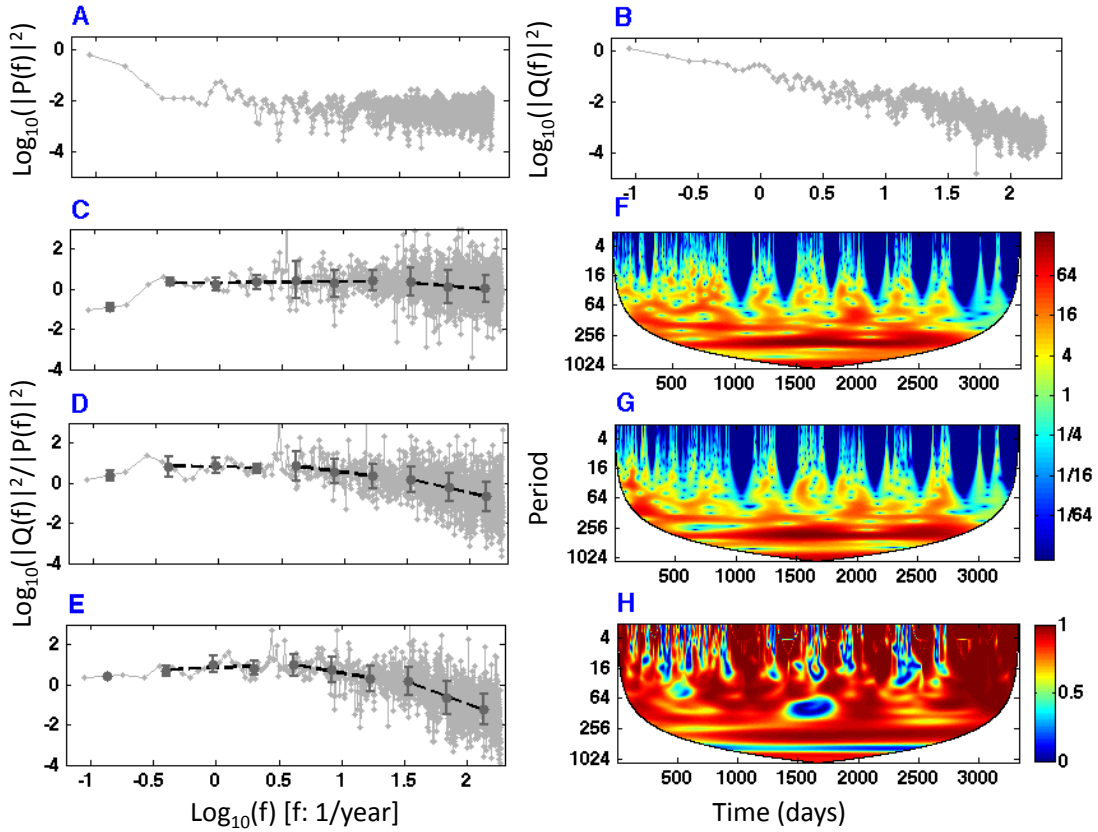


Figure 2. A and B show examples of the power spectra of precipitation and flow at the upper-catchment river station R_5 as a function of frequency (f). Plots C,D and E show the ratio of normalized power spectra (with octave binning) of flow and precipitation as a function of frequency (f) for the three sampling station types (C - surface-flow station; D - tile-flow station; E - river-channel station). Dots show the octave binned values. Error bars indicate the standard deviation within each bin. All power spectra are normalized by the variance (σ^2) of the original timeseries. F and G show examples of continuous wavelet power spectra of standardized timeseries of flow and nitrate concentration respectively for the tile drain station B_1 . Plot H shows the squared wavelet coherence between the standardized flow and nitrate concentration timeseries. White regions correspond to the cone of influence (COI) of edge effects.

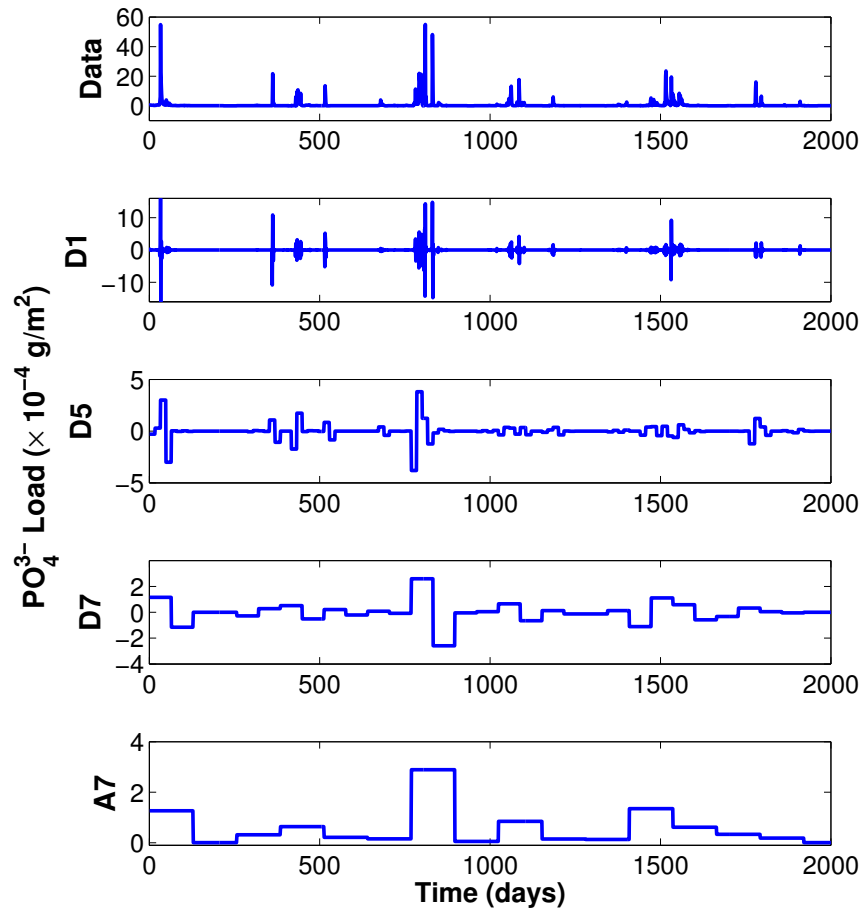


Figure 3. Example of the output of a multi-resolution analysis of L (load-discharge) for PO_4^{3-} . Plots correspond to the raw data ('Data'), the detailed timeseries computed at levels 1, 5 and 7 (which approximately correspond to daily, monthly and seasonal timescales). The lower plot shows the approximation (or smoothed) timeseries computed at seasonal scales.

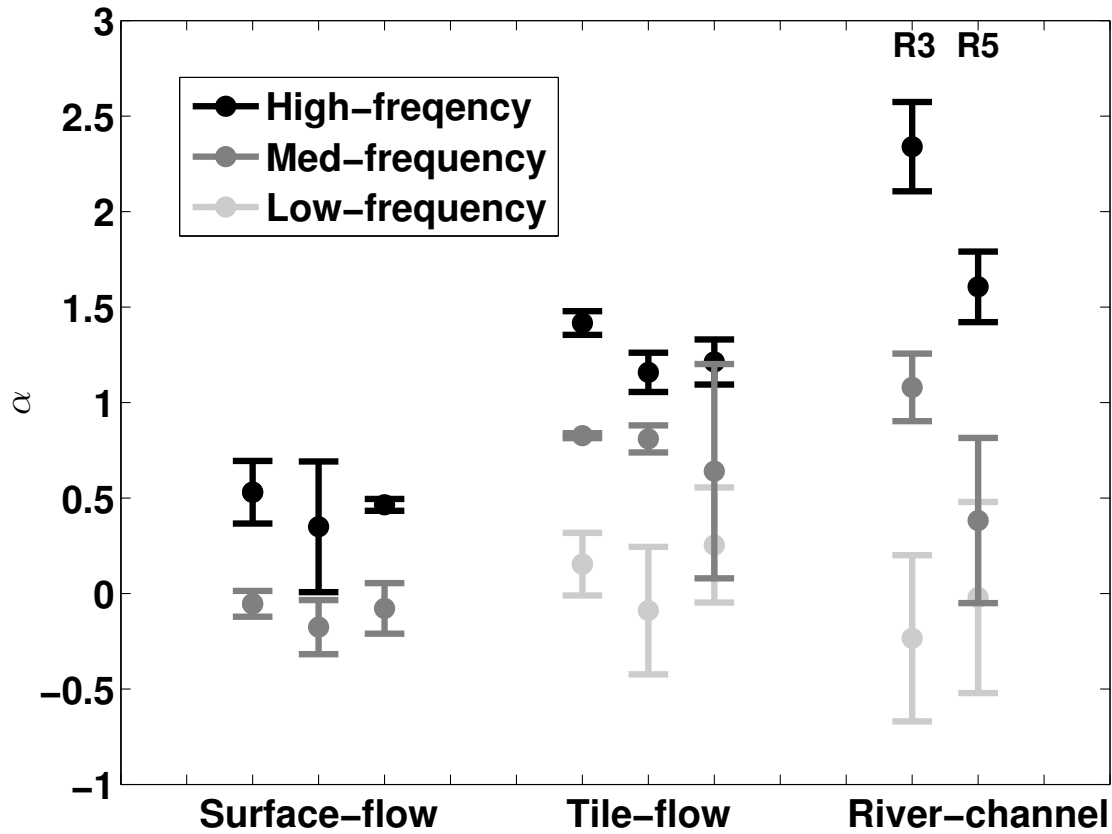


Figure 4. Power law exponents (α) of flow power spectra (normalized by precipitation to isolate the hydrological filter) for the different scaling regimes identified at all sites. The sequence of surface-flow are A2, B2 and C2 from left to right; and A1, B1, and C1 for tile-flow. NO3 indicates nitrate, PO4 phosphate and Atraz indicates atrazine. Error bars indicate the standard error of the fitted exponents. See Table 3 for the location of the scale breaks.

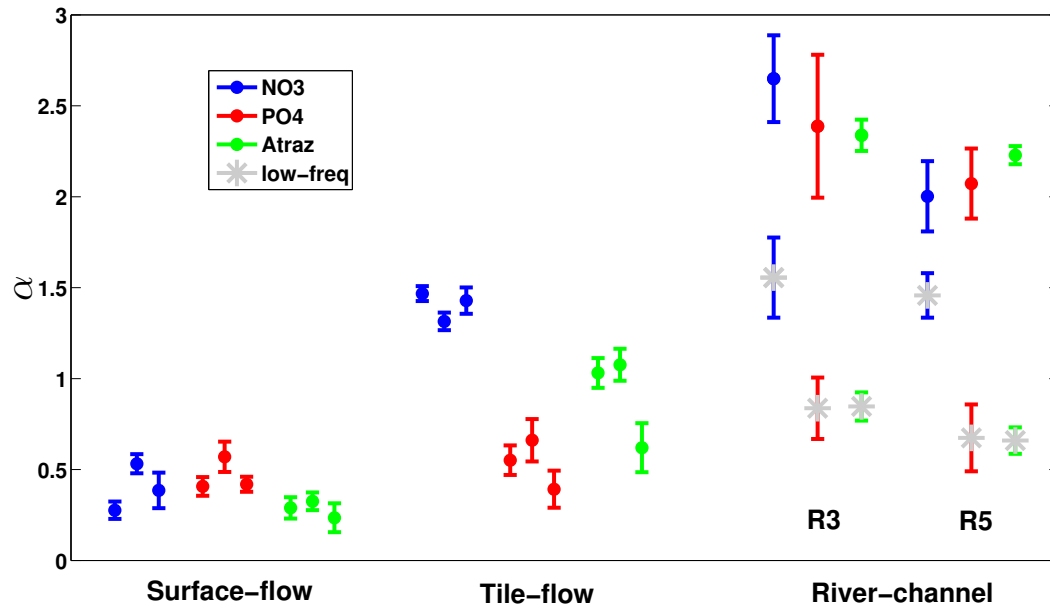


Figure 5. Power law exponents (α) of concentration power spectra for the three chemicals at all sites. Error bars indicate the standard error in the fitted exponents, and scaling breaks are documented in Table 3. The sequence of surface-flow are A2, B2 and C2 from left to right for each chemical; and A1, B1, and C1 for tile-flow for each chemicals.

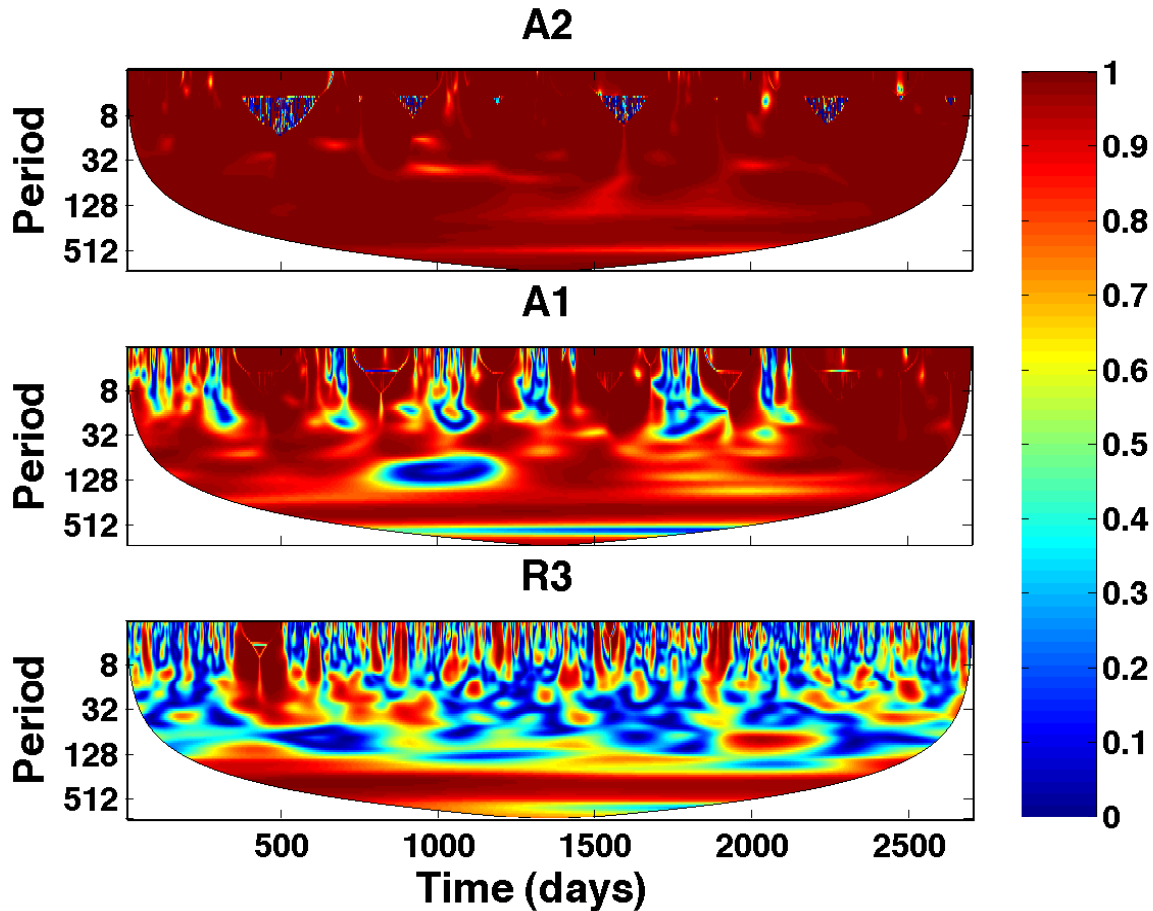


Figure 6. An example of the squared wavelet coherence between the standardized flow and nitrate concentration spectra for three types of sites: a representative surface drain (A_2 , top plot), a tile drain (A_1 , middle plot) and the lower-catchment river station (R_3 , lower plot). Increased complexity and decoupling of discharge and concentration are evident as the spatial scale and dominance of subsurface flow paths increase.

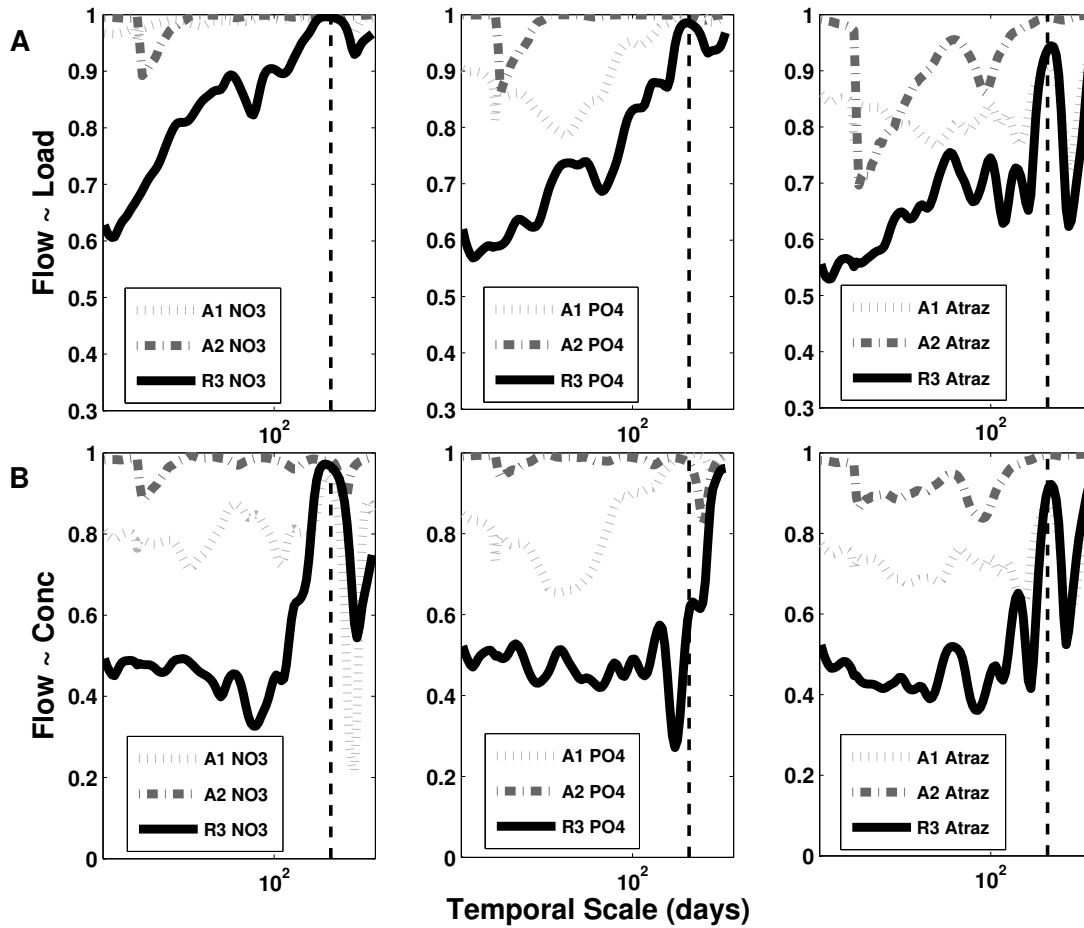


Figure 7. Global squared wavelet coherence between flow and load (A), and between flow and concentration (B), computed as the average across the temporal variability at each frequency (excluding edge effects region COI). The dashed line identifies the annual frequency. NO3 indicates nitrate, PO4 phosphate and Atraz indicates atrazine.

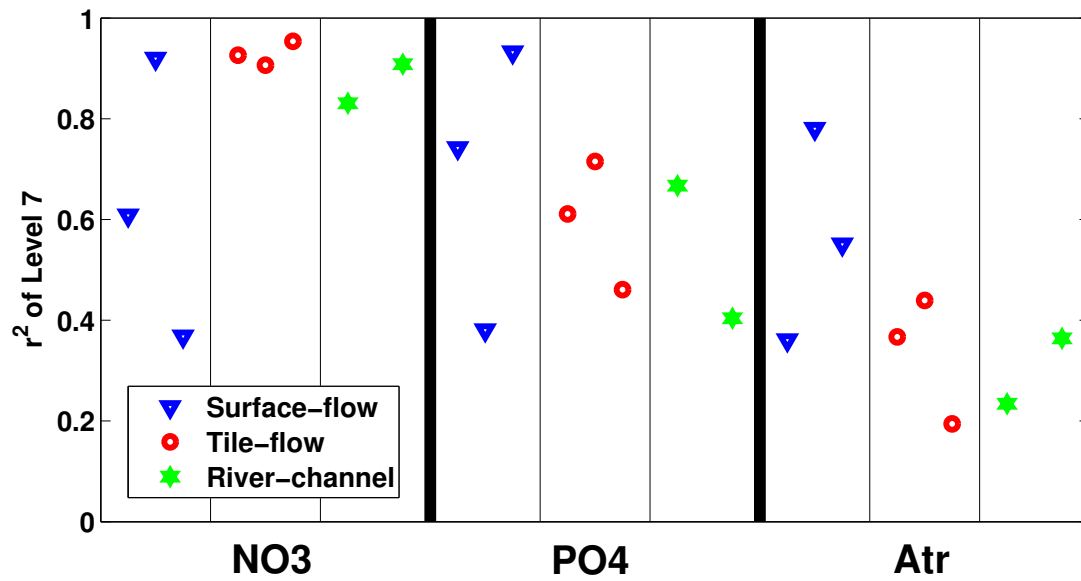


Figure 8. r^2 between filtered L and Q timeseries based on the seasonal approximation (Level 7) from the MRA for all sites and chemicals. The symbol sequence for each chemicals are A2, B2, C2, A1, B1, C1, R3 and R5, from left to right. NO3 indicates nitrate, PO4 phosphate and Atr indicates atrazine.

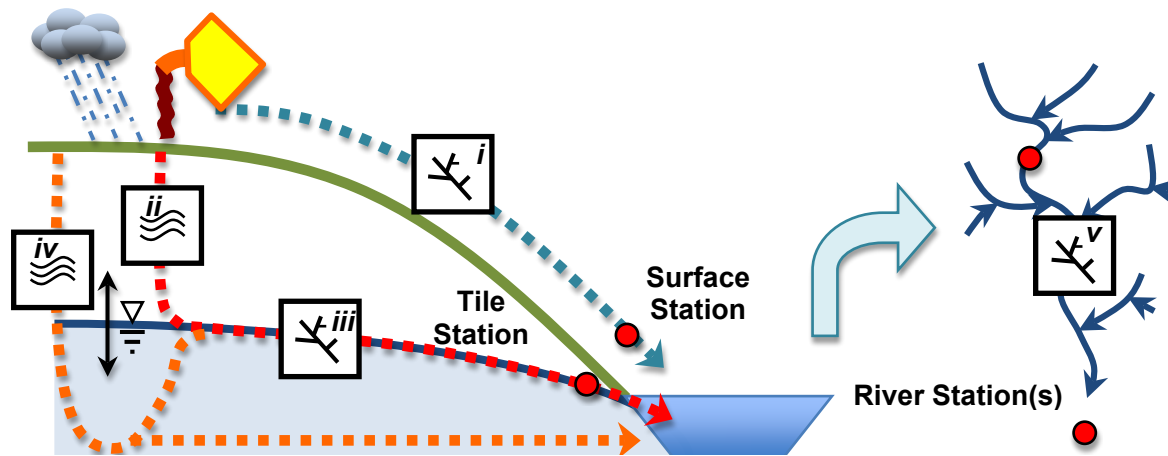


Figure 9. The multiple flow paths and filters in the catchment are indicated on this diagram. Red circles indicate the location of sampling points relative to the flow paths. Network - surface flow ‘filters’ (*i*, *iii* and *v*) are present in the surface drainage networks, the tile drain network and the river network. The properties of these filters vary with scale and with network structure. The vadose zone provides additional filtering (*ii*), which is likely to be stronger for matrix flow and weaker for macropore flow. Vadose zone - water table flow paths (*iv*) provide longer residence times, driven by the timescales of water table response, and consequently the greatest potential for transformation of chemical and hydrological signals. Although 90% of flow in the catchment follows the tile drains, there is potential for the water table to discharge directly to the channels. We do not sample this flow path directly, but its contribution to the river channel is sampled in the river stations. Chemical filtering in (*ii*) and (*iv*) is driven by hydrological transport and chemical availability in these zones. Chemical availability is a function of renewal and removal from transport. The effect of these filters in series is multiplicative and contributes to the appearance of multiple scaling regimes in the Fourier domain.